Koch-Müller, M., Speziale, S., Deon, F., Mrosko, M., Schade, U. (2011): Stress-induced proton disorder in hydrous ringwoodite. - Physics and Chemistry of Minerals, 38, 1, 65-73

DOI: 10.1007/s00269-010-0383-2

Stress-Induced Proton Disorder in Hydrous Ringwoodite

Monika Koch-Müller[1], Sergio Speziale[1], Fiorenza Deon[1], Maria Mrosko[1], Ulrich Schade[2],

[1]Deutsches GeoForschungsZentrum Potsdam, Department 3, Telegrafenberg, 14473 Potsdam

[2]Helmholtz Zentrum BerlinGmbH, Albert-Einstein-Str. 15, 12489 Berlin

Physics and Chemistry of Minerals

DOI 10.1007/s00269-010-0383-2

Abstract

We have measured *in situ* high-pressure IR absorption of synthetic hydrous $(Mg_xFe_{1-x})_2SiO_4$ ringwoodites (x = 0.00 to 0.61) up to a maximum pressure of 30 GPa. In our study, we combined the megabar-type diamond-anvil cell (DAC) with conventional and synchrotron FTIR spectroscopy. The high pressure measurements were performed in three different pressure-transmitting environments: (1) CsI powder, (2) cryogenically loaded liquid argon, and (3) cryogenically loaded liquid argon annealed at 8.6 GPa at temperature of 120°C before further pressure increase. Between 10 and 12 GPa, all the samples loaded with methods (1) and (2), independent on composition, showed a sudden disappearance of the prominent OH–stretching feature and simultaneous discontinuities and/or changes in the pressure dependence of lattice vibrations compared to spectra of samples loaded with method (3). In experiments performed with method (3) the OH stretching vibrations as well as lattice vibrations could be observed up to 30 GPa and their pressure behaviour ($d\nu/dP$) can well be described by linear fits. Molecular vibrations, such as the OH stretching, are very sensitive to non-hydrostatic conditions, especially in minerals with highly symmetric structures. We interpret the disappearance of the OH-bands using method (1) and (2) as a stress-induced proton disordering in hydrous ringwoodite. Our results confirm that argon pressure medium produces strongly non-hydrostatic conditions comparable to CsI or KBr, if it is not thermally annealed at pressures above 8 GPa. Our results suggest that the transition observed in hydrous Mg-ringwoodite endmember is not present in compositions containing Fe. By comparing the behavior of samples compressed in very different environments, we suggest that sudden disappearance of the OH stretching band in hydrous ringwoodite could be driven by deterioration of the quasi-hydrostatic stress condition instead of a pressure-induced effect.

Keywords Ringwoodite - Diamond-anvil cell - Infrared spectroscopy - Synchrotron - Pressure-transmitting medium

Introduction

Olivine, wadsleyite and ringwoodite, the three polymorphic modifications of $(Fe,Mg)_2SiO_4$, have been the subject of numerous studies in the past to determine the maximum solubility of hydrogen in their structures (e.g., Kudoh et al. 2000). Nowadays experimental work is more focused on the effect of hydrogen incorporation on the physical, structural and thermodynamic properties (e.g. Jacobsen et al. 2004, Inoue et al. 2004, Litasov and Ohtani 2007). A systematic knowledge of the compositional dependence of the physical properties of $(Fe,Mg)_2SiO_4$ polymorphs can allow us to make substantial progresses in the interpretation of the fine details of seismic data relative to the upper mantle and transition zone and to understand the mechanism of water recycling in the deep Earth (Bercovici and Karato, 2003; van der Meijde et al., 2003; Blum and Shen, 2004; Hirschmann et al., 2005; Huang et al., 2005; Suetsugu et al., 2006).

Chamorro Pérez et al. (2006) studied hydrous Mg-ringwoodite (1 and 1.7 wt % water) by in-situ high-pressure IR spectroscopy up to 30 GPa using neon as pressure medium and reported a second-order phase transition at pressures of about 25 GPa visible as a sudden disappearance of the prominent OH band centered at 3150 cm^{-1}. The results of Chamorro Pérez and coauthors support previous observations of additional Raman features in hydrous Mg-ringwoodite at pressures above 30 GPa (Kleppe et al. 2002a). In a separate study Kleppe et al. (2002b) performed a high-pressure Raman study of hydrous Mg_{89}-ringwoodite. The interpretation of the results of this study are however controversial, and do not confirm the presence of a similar transition in Fe-containing ringwoodite (Kleppe and Jephcoat, 2006).

In order to systematically investigate the effect of pressure on the local arrangement of hydrogen in more Fe-rich $(Fe,Mg)_2SiO_4$ compositions we synthesized hydrous ringwoodite of different compositions ranging from x_{Mg}= 0.00 to x_{Mg}= 0.61 and collected insitu MIR spectra as a function of pressure in the OH stretching range as well as in the range of the lattice vibrations.

Experimental methods

Sample characterization

Hydrous ringwoodite with five different iron contents (Tab. 1) were synthesized in a multi-anvil apparatus and characterized by electron microprobe analyses (EMPA) and secondary ion mass spectrometry (SIMS). Details of the experimental procedures and results of EMPA are given in Taran et al. (2009) and Koch-Müller et al. (2009); details of the SIMS measurements are given in Koch-Müller and Rhede (2010).

FTIR spectroscopy

All samples were investigated by FTIR spectroscopy (using conventional and/or synchrotron radiation) at ambient condition and four of them (MA-62, -68, -120, -121) in-situ up to 30 GPa in a diamond anvil cell (DAC). For the conventional FTIR spectroscopy we used a Bruker IFS 66v FTIR spectrometer connected to a Hyperion microscope using a Globar as light source, a KBr beamsplitter and InSb (NIR) and MCT (MIR) detectors. The spectra were collected with a resolution of 2 cm^{-1}, averaged over 1024 scans and with apertures of about 50 by 70 µm. Spectra of samples smaller than 50 µm were obtained at the synchrotron IR-beamline of the Helmholtz Zentrum Berlin GmbH (former BESSY II) using a Nicolet 870 spectrometer with KBr beamsplitter equipped with a continuum microscope, a MCT detector and apertures of about 30 by 40 µm. The brilliant synchrotron light enables us to reduce the spectra collection time of a factor 4 with a much better signal to noise ratio. We used in all cases a megabar-type symmetric piston-cylinder DAC (MaO and Hemley, 1998) with Type II diamonds with culet size of 600 µm and pre-indented stainless steel gaskets with a 300 µm hole. The spectra were collected in the spectral range 4000 - 450 cm^{-1} on single crystals and/or thin films produced by compressing the powdered sample in a non-gasketed DAC. We compressed our samples in three different pressure-transmitting environments: (1) CsI

powder; (2) cryogenically loaded liquid argon, (3) cryogenically loaded liquid argon annealed at 8.6 GPa to 120°C (by placing the DAC in an oven for one hour) before further increasing the pressure to ensure more hydrostatic conditions (Wittlinger et al. 1997). For the cryogenic loading we followed the procedure described in Wittlinger et al. (1997): the sample-loaded diamond-anvil cell was placed still open in a box, which was cooled with liquid nitrogen from outside. Then liquid argon was poured into the box until the cell was completely drowned in argon. The cell was then closed and heated up to room temperature. To avoid impurities of oxygen or nitrogen the box was purged with argon gas for about 5 min before we filled it with liquid argon. The initial pressure, after cryogenic argon loading, always exceeded 1.2 GPa therefore argon was already solid when the diamond-anvil cell was equilibrated at room temperature. Wittlinger et al. (1997) showed by X-ray diffraction that using argon as pressure medium X-ray reflections of materials in the cell broaden at 8.5 GPa by a factor of 5 compared with those measured at 1.6 GPa. They linked this observation to non-hydrostaticity of the crystalline argon. At higher pressures the situation became even worse. However, they found that this effect can be completely reversed by heating the whole cell at 8.6 GPa to 120°C°C for several hours - during this process argon recrystallizes, the pressure gradient disappears and reflections become sharp again. In our case the pressure gradient under non-hydrostatic condition (without annealing) was about ± 0.05 GPa below 8 GPa, ± 0.1 GPa at about 10 GPa and as high as ± 1.0 GPa at 20 GPa. As pressure increased also the ruby fluorescence lines broaden. However after annealing at 8.6 GPa the ruby lines become sharp again and the pressure gradient was much less than in the non-annealed experiments of about ± 0.2 GPa even at the highest pressure of 30 GPa.

The spectra were fitted with the program PeakFit by Jandel Scientific using the 2nd derivative zero algorithm for the background and mixed Gaussian and Lorenzian distribtuion function for the component bands. Some of the high-pressure spectra suffered from strong interference

fringes between the culets of DAC - these were either removed by the method given in Neri et al. (1987) (see Fig. 2) or they were deconvoluted with the PeakFit software together with the bands resulting from the sample.

Results

Water determination using SIMS in combination with IR spectroscopy yielded concentrations ranging from 0.21 wt % for the Fe- endmember to 0.36 wt % for the Mg-richest sample (x_{Mg} = 0.61). Fig. 1 shows IR spectra collected in the OH – stretching region on single crystals in-situ in a DAC loaded with method (1) and (2). The OH band in spectra of the most Mg-rich sample (MA-121) shifts from 3244 cm^{-1} at ambient conditions to about 3200 cm^{-1} at 10.3 GPa while in the spectra of the more Fe-rich sample (MA-62) the shift is stronger: from 3260 cm^{-1} at ambient condition to 3140 cm^{-1} at 10.1 GPa. Between 10 and 12 GPa a sudden disappearance of the prominent OH feature can be observed, however independent on composition (x_{Mg}) and water content. Fig. 2a shows MIR spectra of ringwoodites with three different compositions. Depending on the sample thickness the MIR spectra show overtones and combination modes of fundamental modes (crystals or films > 20 μm) (Fig. 2a and 3) or only the fundamental modes ν_3 and ν_4 (thin films) (Fig. 2 and 4). Table 2 summarize the observed bands and band assignments following the suggestions of Chopelas et al. (1994) and Hofmeister and Mao (2001). In the same pressure range at which the OH band disappears we observe discontinuities in the lattice vibration region (Fig. 2, 3 and 5). However, applying method (3) the OH stretching vibrations as well as lattice vibrations can be observed up to 30 GPa without any discontinuity and their pressure behaviour (dν/dP) can well be described by linear fits (Fig. 4 and 5). The discontinuities in the pressure behavior are more pronounced for the modes shown in Fig. 5 c and d. The trends of the modes ν_3 and ν_4 (Fig. 5a) can also be modelled with a gently curving trend without discontinuity - however in any case this is different to the behavior of the sample in the annealed experiments. The fitted slopes from the

linear regressions from the annealed experiments (r^2 = 0.99 in both cases) for ν_3 and ν_4 are 3.731 and 2.281 cm^{-1}/GPa, respectively (see Fig. 5b). Calculated mode Grüneisen parameters $\gamma_i = -(\partial \ln \nu_i / \partial V)_T = K_T(\partial \ln \nu_i / \partial P)_T$ (where ν is frequency, K is the bulk modulus, the subscript i refers to the i^{th} infrared mode, the subscript T refers to isothermal conditions) using a bulk modulus of 187(2) GPa (Nestola et al. 2010) are 0.83(2) for ν_3 and 0.81(2) for ν_4.

Discussion

We performed repeated DAC experiments with hydrous ringwoodite of different compositions in combination with MIR spectroscopy using different pressure-transmitting environments in order to evaluate the effects of non-hydrostatic conditions on the local behavior of OH groups in the structure of Fe-rich compositions in the ringwoodite. It has been demonstrated that ringwoodite is very sensitive to both Fe/Mg substitution and hydrogen incorporation with a net decrease of 14% of the shear modulus by combined 11% Fe/Mg substitution and 1% water incorporation (Jacobsen and Smyth, 2006).

We compared the MIR high pressure spectra obtained using the relatively hard pressure-transmitting media CsI powder and cryogenically loaded liquid argon (pressure-transmitting environment 1 and 2, respectively; see the experimental method section) to spectra obtained using cryogenically loaded liquid argon which was annealed for one hour at 8.6 GPa to 120°C (pressure-transmitting environment 3) before we further increased pressure. Wittlinger et al. (1997) show that this procedure ensures more quasi-hydrostatic conditions at pressure above 10 GPa compared to the experiments performed in argon pressure medium without thermal annealing. In the experiments performed using pressure-transmitting environments (1) and (2) the prominent OH-stretching bands suddenly disappear between 10 and 12 GPa independent on composition, and the lattice vibrations show discontinuities and/or different trends with pressure compared to experiments using enviroments (3). In experiments using pressure-

transmitting environment (3) the OH stretching vibrations as well as lattice vibrations could be observed up to 30 GPa without any discontinuity and their pressure behaviour can be well described by linear fits.

The slopes (dν/dP) for ν_3 (3.731 cm^{-1}/GPa) and ν_4 (2.281 cm^{-1}/GPa) for MA-120 are comparable to those provided by Hofmeister and Mao (2001), i.e. 3.988 (ν_3) and 1.370 (ν_4) for γ-Mg_2SiO_4 and 4.500 (ν_3) and 1.541 (ν_4) for the Fe-endmember. The mode Grüneisen parameters for our internal Si-O modes are in the expected range (less than 1.0) for the stiff Si polyhedra (Hofmeister et al. 1989). Interestingly, for olivine the average γ_i for the internal modes is 0.46 (Hofmeister et al., 1989), but for wadsleyite it is about 0.75 (Cynn and Hofmeister 1994), which is 8 to 10 % less than our values for Fe-rich ringwoodite. In all experiments the pressure-induced effects were completely reversible. The quantitative analysis of the spectra of the recovered samples in the OH stretching region always shows that the OH content is preserved. Thus, the disappearance of the OH band must be interpreted as an extreme broadening of the OH band which in turn can be linked to a high degree of hydrogen disorder with a large range of O-H....O distances. As this behaviour only occurs in the pressure environments (1) and (2) which are known to produce strong non-hydrostatic conditions, we interpret the disappearance of the OH-bands as a stress-induced proton disorder in hydrous ringwoodite due to the use of hard pressure-transmitting media like CsI or argon without thermal annealing. In addition to the proton disorder we observe discontinuities in the band shifts with pressure for the Si-O stretching and bending fundamental modes ν_3 and ν_4 and their combinations and overtones when using hard pressure-transmitting media. The translation modes of the octahedral cations seem to be unaffected by the non-hydrostatic conditions.

Salts as pressure media such as KBr or CsI are easy to load and transparent in the infrared but they are known for producing strongly non-hydrostatic conditions. The same is true for argon

at pressure above few GPa without thermal annealing (Bell and Mao 1981; Angel et al., 2007; Klotz et al., 2009). Molecular vibrations are very sensitive to non-hydrostatic conditions. The results of spectroscopic investigations of materials with high symmetry such as ringwoodite show that they are very sensitive to small uniaxial components in the pressure (Sherman and Stadtmuller 1987). In addition, the OH stretching vibrations in general are very sensitive to non-hydrostatic conditions if compared to M-O stretching vibrations.

Our results for hydrous Fe-rich ringwoodite strengthen our previous observation in repeated experiments in the OH stretching region of olivine spectra (Koch-Müller et al., 2006). In that study we made the following observations: the OH bands in the range of 3612 - 3566 cm^{-1} shift with increasing pressure from ambient conditions to 10 GPa to higher energies when using KBr as pressure medium (Koch-Müller et al., 2006) but taking the same sample they shift significantly to lower energies when the cell was cryogenically loaded with liquid argon without annealing (Fig. 6). In this case the spectra taken with argon as pressure-transmitting medium may give the true behaviour, but the pressure behavior in the KBr experiments must be induced by stress. These observations are contradicting those by Hofmeister et al. (1989), who did not observe differences in the pressure behaviour of the olivine mid - far IR bands in strongly non-hydrostatic conditions compared to quasi-hydrostatic conditions. This may indicate that the lattice vibrations of olivine are less sensitive to non-hydrostatic conditions than OH bands.

Our study shows that in quasi-hydrostatic conditions hydrous Fe-containing ringwoodite compositions do not present the transition observed by Chamorro Pérez et al. (2006) in hydrous ringwoodite compressed in neon pressure-transmitting medium. However, a behavior qualitatively very similar to that observed by Chamorro Pérez et al. can be induced in our sample by substantial uniaxial stress development in the sample chamber (due to freezing of the pressure medium). The use of neon as pressure-transmitting medium guarantees quasi-hydrostatic conditions up to pressures in excess of 10 GPa (Klotz et al., 2009). Nevertheless

in the pressure regime above 20 GPa neon becomes sensibly non-hydrostatic (Bell and Mao, 1981; Klotz et al., 2009) if it is not thermally annealed. For this reason we argue that their observation of a sudden disappearance of the OH band may also be related to non-hydrostatic conditions.

Figure captions

Fig. 1: MIR spectra showing OH-bands of ringwoodite as a function of pressure using either argon or CsI as pressure medium without annealing. The spectra are offset for clarity. The numbers attached to each spectrum correspond to the experimental pressure in GPa.

Fig. 2: a. MIR spectra of samples: MA-75 (3 upper lines) taken on a single crystal and on films of different thicknesses; MA-62 taken on a single crystal; MA-68 (bottom) taken on a thin film and on a single crystal. b. MIR spectrum of a thin film of sample sample MA-120 as a function of pressure with interference fringes from the DAC; c. after elimination of the fringes according to the method given in Neri et al. (1987).

Fig. 3: MIR spectra (fundamentals and overtones) of ringwoodite as a function of pressure a., c. and d. using synchrotron radiation and b. using a globar light source. The spectra are offset for clarity. The numbers attached to each spectrum correspond to the experimental pressure in GPa.

Fig. 4: MIR-bands of ringwoodite MA-120 in the OH stretching region (a) and in the region of the lattice vibration (b) as a function of pressure using argon as pressure medium and following the procedure of Wittlinger et al. (1997). The spectra are offset for clarity. The numbers attached to each spectrum correspond to the experimental pressure in GPa. The sharp bands around 3000 cm^{-1} result from hydrocarbon contamination (C-H stretching).

Fig. 5: Shifts of the IR vibrational bands of ringwoodite as function of pressure a.c. and d. using argon as pressure medium without annealing; b. using argon and following the procedure of Wittlinger et al. (1997).

Fig. 6: IR spectra of synthetic (6 GPa/1100°C) hydrous olivine as a function of pressure taken in the OH stretching region a. using KBr as pressure medium; b. using argon as pressure medium without annealing. The spectra are offset for clarity. The numbers attached to each spectrum correspond to the experimental pressure in GPa.

References

Angel RJ, Bujak M, Zhao J, Gatta GD, Jacobsen SD (2007)Effective hydrostatic limits of pressure media for high-pressure crystallographic studies. J. Appl. Cryst., 40: 26-32

Bell PM, Mao HK (1981) Degrees of hydrostaticity in He, Ne and Ar pressure-transmitting media. Carnegie Inst Wash Yrbk 80: 404-406

Bercovici D, Karato SI (2003) Whole mantle convection and transition-zone water filter. Nature, 425: 39-44

Blum J, Shen Y (2004) Thermal, hydrous and mechanical states of the mantle transition zone beneath southern Africa. Earth Planet. Sci. Lett. 217: 367-378

Chamorro Pérez EM, Daniel I, Chervin JC, Dumas P, Bass JD, Inoue T (2006) Synchrotron IR study of hydrous ringwoodite (γ−Mg_2SiO_4) up to 30 GPa. Phys Chem Miner 33: 502 – 510

Chopelas A, Boehler R, Ko T (1994) Thermodynamics and behavior of γ-Mg_2SiO_4 at high pressure: Implication for Mg_2SiO_4 phase equilibrium. Phys Chem Miner 21:351-359

Cynn H, Hofmeister AM (1994) High-pressure IR spectra of lattice modes and OH vibrations in Fe-bearing wadsleyite. Jour Geophys Res 99: 17717–17727

Hirschmann MM, Aubaud C, Withers AC (2005) Storage capacity of H_2O in nominally anhydrous minerals of the upper mantle. Earth Planet. Sci. Lett., 236: 167-181

Hofmeister AM, Mao HK (2001) Evaluation of shear moduli and other properties of silicates with the spinel structure from IR spectroscopy. Am Min 86: 622–639

Hofmeister AM, Xu J, Mao HK, Bell PM, Hoering TC (1989) Thermodynamics of Fe-Mg olivines at mantle pressures: mid- and far-infrared spectroscopy at high pressure. Am Min 74: 281–306

Huang X, Xu Y, Karato SI (2005) Water content of the mantle transition zone from the electrical conductivity of wadsleyite and ringwoodite. Nature, 434: 746-749

Inoue T, Tanimoto Y, Irifune T, Suzuki T, Fukui H, Ohtaka O (2004) Thermal expansion of wadsleyite, ringwoodite, hydrous wadsleyite and hydrous ringwoodite. Phys Earth Plan Int 143-144: 279–290

Jacobsen SD, Smyth JR, Spetzler H, Holl CM, Frost DJ (2004) Sound velocities and elastic constants of iron-bearing hydrous ringwoodite. Phys Earth Plan Int 143: 47–56

Jacobsen SD, Smyth JR (2006) Effect of water on the sound velocities of ringwoodite in the transition zone. In Earth's Deep Water Cycle, AGU Geophys. Monogr. Ser., 168: 131-145

Kleppe AK, Jephcoat AP, Smyth JR (2002a) Raman spectroscopic study of γ-Mg2SiO4 ringwoodite to 56.5 GPa. Phys. Chem. Minerals, 29: 473-476

Kleppe AK, Jephcoat AP, Smyth JR, Frost DJ (2002b) On protons, iron and the high pressure behavior of ringwoodite. Geophys. Res. Lett., 29: doi:10.1029/2002GL015276

Kleppe AK, Jephcoat AP (2006) Raman spectroscopic studies of hydrous and nominally anhydrous deep mantle phases. In Earth's Deep Water Cycle, AGU Geophys. Monogr. Ser., 168: 69-93

Klotz S, Chervin J-C, Munsch P, Le Marchand G (2009) Hydrostatic limit of 11 pressure transmitting media. J. Phys. D: Appl. Phys., 42: 075413

Koch-Müller M, Matsyuk SS, Wirth R (2006) Hydrogen incorporation in olivine: Nature versus experiments, 11th International Conference on Experimental Mineralogy, Petrology and Geochemistry (Bristol, UK 2006) 39

Koch-Müller M, Rhede D, Schulz R, Wirth R (2009) Breakdown of hydrous ringwoodite to pyroxene and spinelloid at high P and T and oxidizing conditions. Phys Chem Min 36: 329–341

Koch-Müller M, Rhede D (2010) IR absorption coefficients for water in nominally anhydrous high-pressure minerals. Am Mineral 95:770–775

Kudoh Y, Kuribayashi T, Mizohata H, Ohtani E, (2000) Structure and cation disorder of

hydrous ringwoodite Phys Chem Min 27: 474–479

Litasov KD, Ohtani E (2007) Effect of water on the phase relations in Earth's mantle and deep water cycle. Special Paper - Geological Society of America 421: 115–156

Mao HK, Hemley RJ (1998) New window on the earth's deep interior. In Hemley RJ Ed: Ultrahigh Pressure Mineralogy 37: 1-32. Reviews in Mineralogy, Mineralogical society of America, Washingon D.C.

Neri F, Saitta G, Chiofalo S (1987) A simple procedure to remove the interference fringes from optical spectra. J Phys E: Sci Instrument 20: 894–896

Nestola F, Boffa Ballaran T, Koch-Müller M, Balic-Zunic T, Taran M, Olsen L, Prinivalle F, Secco L (2010) New accurate elasticity data for Fe_2SiO_4 ringwoodite. Physics Earth Planetary Interiors (in press)

Sherman WF, Stadtmuller AA (1987) Experimental techniques in high-pressure research. John Wiley & Sons LTD, Chichester, New York, Brisbane, Toronto, Singapure, p.471

Suetsugu D, Inoue T, Yamada A, Zhao D, Obayashi M (2006) Towards mappng the three-dimentional distribution of water in the transition zone form P-velocity tomography and 660-km discontinuity depths. In: Steven D. Jacobsen, Suzan van der Lee (eds) "Earth's deep water cycle. Geophysical monograph series 168", AGU. pp. 237-249

Taran M, Koch-Müller M, Wirth R, Abs-Wurmbach I, Rhede D, Greshake A. (2009) Spectroscopic studies of synthetic and natural ringwoodite, γ-$(Mg, Fe)_2SiO_4$. Phys Chem Min 36: 217–232

van der Meijde M, Marone F, Giardini D, van der Lee S (2003) seismic evidence for water in the Earth's upper mantle. Science, 300: 1556-1558

Wittlinger J, Fischer R, Werner S, Schneider J, Schulz H (1997) High-pressure study of h.c.p.-Argon. Acta Cryst B53: 745–749

Table 1: Some characteristics of the synthetic ringwoodite samples

Sample No	x_{Mg}	H_2O wt. %	wavenumber cm^{-1} ambient	wavenumber cm^{-1} (at P in GPa)
MA-75	0.00	0.21(1) [a]	3386	-
MA-62	0.39	0.30(2) [a]	3260	3140 (10.1)
MA-68	0.50	0.32(5) [b]	3252	-
MA-120	0.60	0.36(3) [a]	3244	3102 (31.7)
MA-121	0.61	0.36(5) [b]	3244	3198 (10.3)

[a] SIMS measurements (Koch-Müller and Rhede, 2010)

[b] IR-spectroscopic

Table 2: IR fundamental modes and overtones of ringwoodite (cm^{-1})

Mode	γ-Fe_2SiO_4 H+M (2001)[a]	γ-Fe_2SiO_4 MA-75	γ-$Mg_{0.8}Fe_{1.2}SiO_4$ MA-62	γ-$Mg_1Fe_1SiO_4$ MA-68	γ-$Mg_{1.2}Fe_{0.8}SiO_4$ MA-120	γ-Mg_2SiO_4 H+M (2001)[a]
DAC experiments			CsI, syn[b] Ar n.a., syn[b] 2 × CsI, Globar[b]	Ar n.a., syn[b] CsI, Globar[b]	Ar, n.a, Globar[b] 2 × Ar, a., Globar[b]	
2 ν_3	1594	1595	1603	1606		1622
$2\nu_4$	978		1010			1086
ν_3 + T(M)	1093					1221
ν_4 + T(mix) + LA	889	1031				1127
ν_4 +T(mix)+TA	796		972[b]	1013[b]		1038
ν_3	797	832[c]			830[b,c]	811
ν_4 + T(mix)	689		753			894
ν_4 + LA	689	689	733[b]			796
T(M)+ T(mix)	488		718[b]	720[2]		760
2 T(M)	600	583	654[b]	657		820
2 T(mix)	370		583			702
ν_4	489	499		519	521[b,c]	543
T(M)	296		341[d]	353[d]	364[d]	410
T(mix)	200					351
LA	200					253
TA	107					144

[a] TO modes taken from Hofmeister and Mao (2001)

[b] From DAC experiments: CsI as pressure medium; *syn*: using synchrotron radiation, *Ar, n a.* using Argon as pressure medium with no annealing; *Ar, a*. using Argon as pressure medium with annealing (Wittlinger et al., 1997)

[c] The fundamental mode in our spectra are very broad and asymmetric and the peak position is hard to define exactly. Weather the broadness and asymmetry is related to the water content will be the subject of further investigations.

[d] linear extrapolation of the endmember modes

Notes: ν_3 Si-O tetrahedral stretch; ν_4 O-Si-O tetrahedral bend; *T(M)* translation of octahedral cations; *T(mix)* translation of both octahedral and tetrahedral cations (Chopelas et al., 1994)

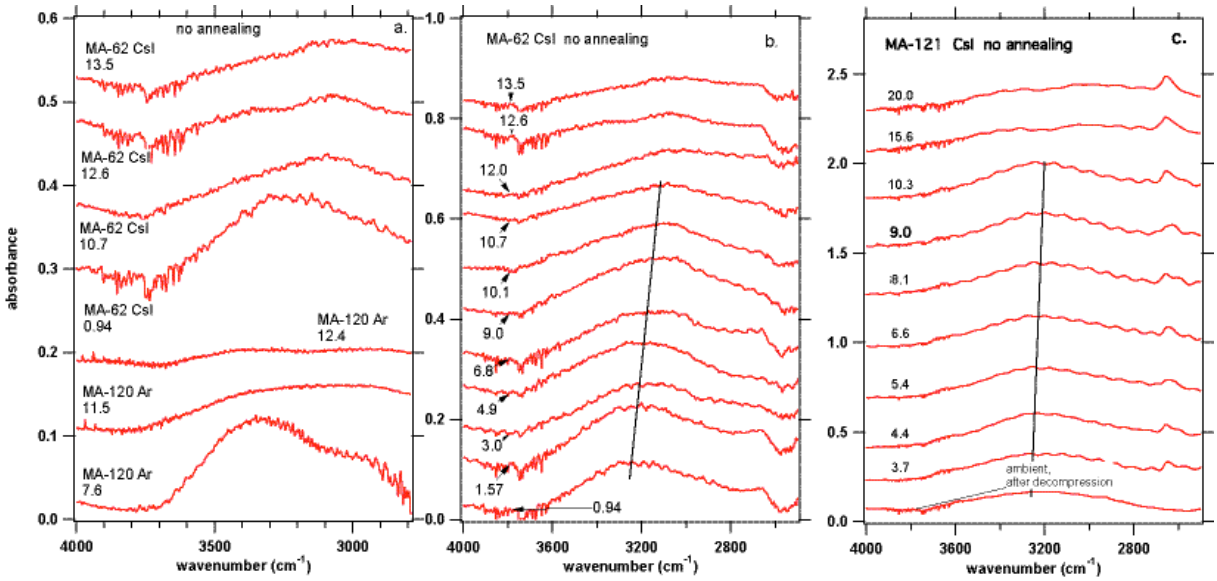
no annealing
a.
MA-62 CsI
13.5
MA-62 CsI
12.6
MA-62 CsI
10.7
MA-62 CsI
0.94
MA-120 Ar
12.4
MA-120 Ar
11.5
MA-120 Ar
7.6
absorbance
wavenumber (cm-1)
MA-62 CsI no annealing
b.
13.5
12.6
12.0
10.7
10.1
9.0
6.8
4.9
3.0
1.57
0.94
wavenumber (cm-1)
MA-121 CsI no annealing
c.
20.0
15.6
10.3
9.0
8.1
6.6
5.4
4.4
3.7
ambient,
after decompression
wavenumber (cm-1)

Fig. 1

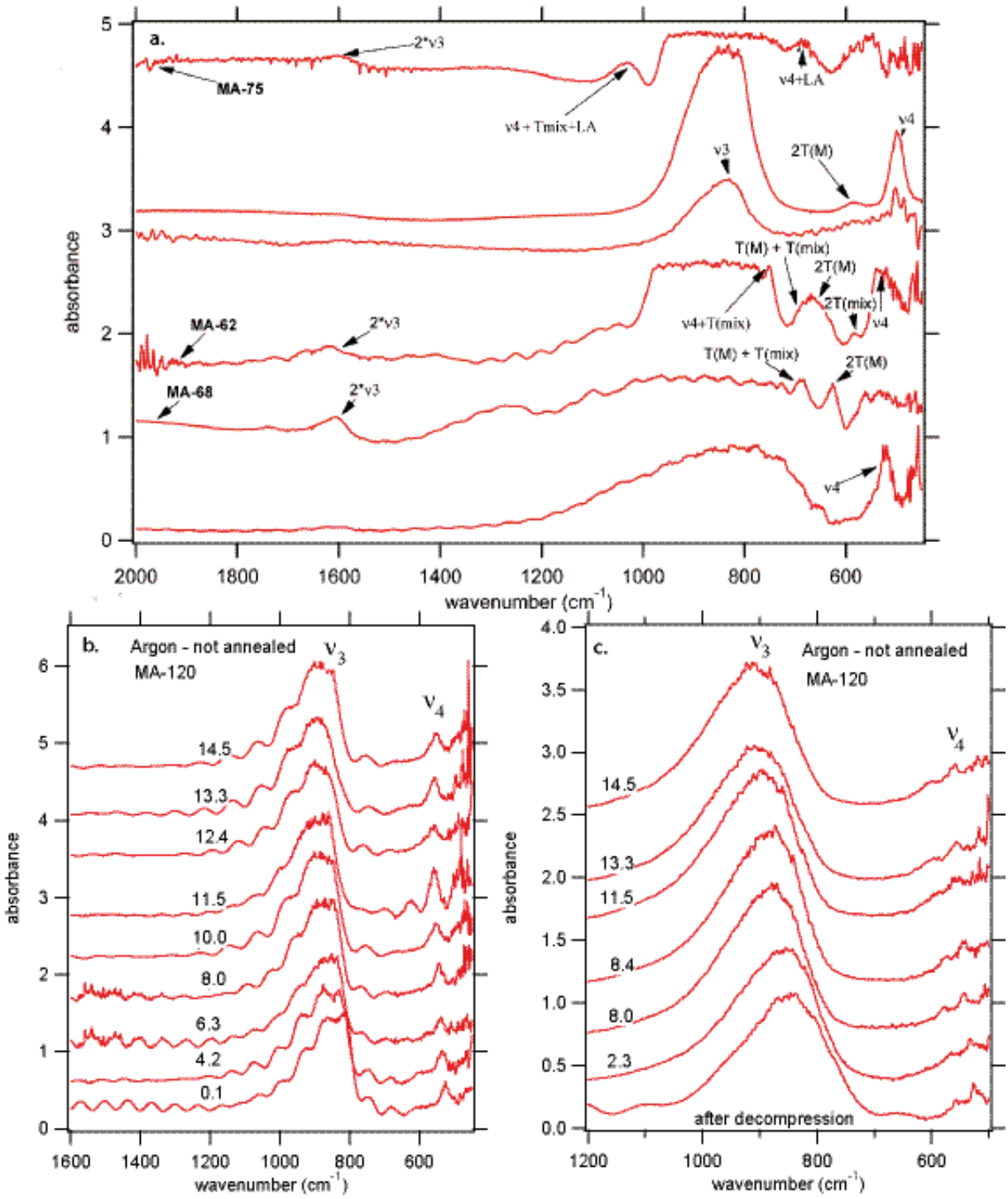
a.
MA-75
2*v3
v4+LA
v4+Tmix+LA
v4
v3
2T(M)
T(M) + T(mix)
2T(M)
2T(mix)
v4
v4+T(mix)
MA-62
2*v3
T(M) + T(mix)
2T(M)
MA-68
2*v3
v4
absorbance
wavenumber (cm-1)
b.
Argon - not annealed
MA-120
ν3
ν4
14.5
13.3
12.4
11.5
10.0
8.0
6.3
4.2
0.1
absorbance
wavenumber (cm-1)
c.
ν3
Argon - not annealed
MA-120
ν4
14.5
13.3
11.5
8.4
8.0
2.3
after decompression
absorbance
wavenumber (cm-1)

Fig. 2

Fig. 3

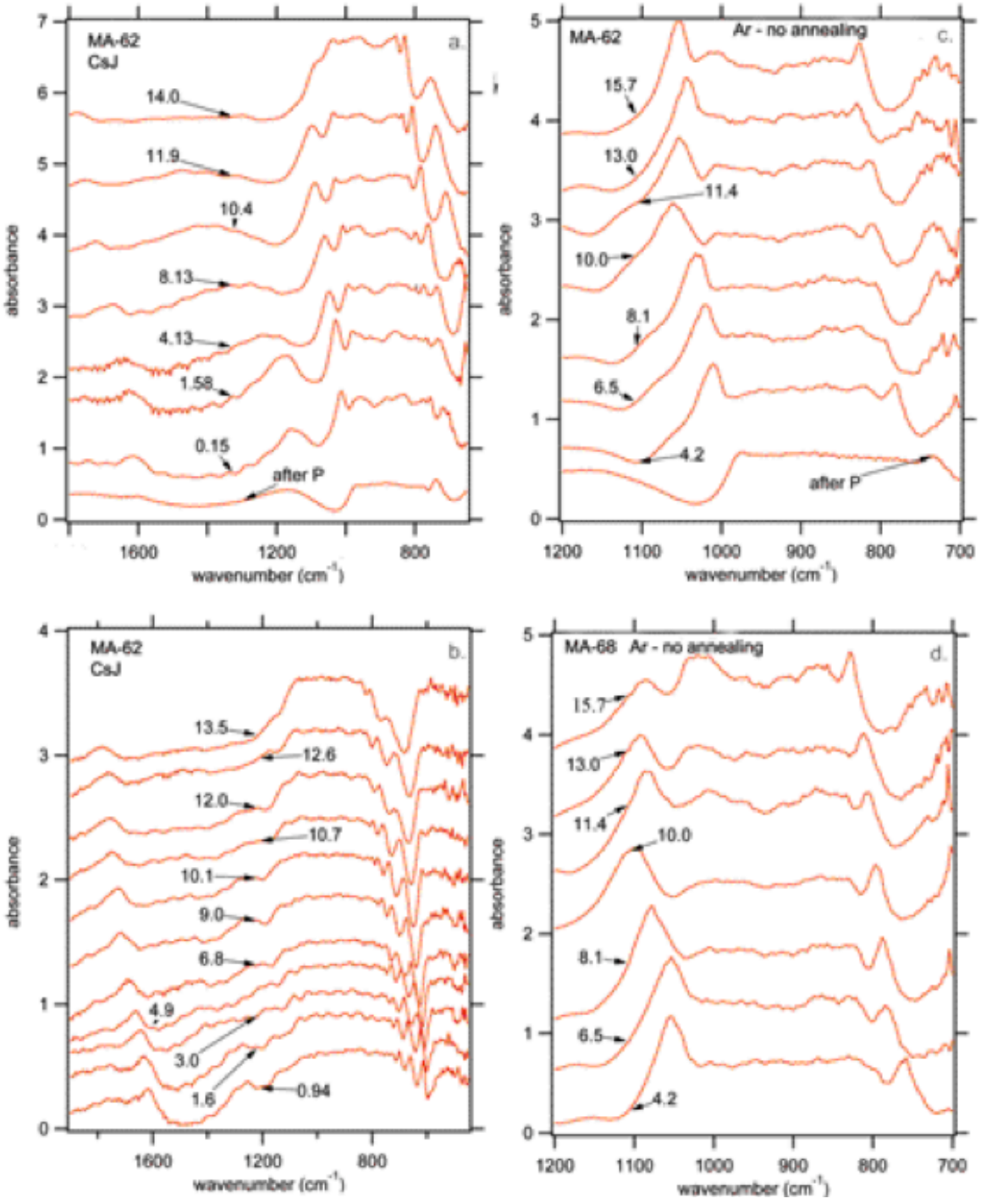
MA-62
CsJ
a.
14.0
11.9
10.4
8.13
4.13
1.58
0.15
after P
absorbance
wavenumber (cm-1)
MA-62
Ar - no annealing
c.
15.7
13.0
11.4
10.0
8.1
6.5
4.2
after P
absorbance
wavenumber (cm-1)
MA-62
CsJ
b.
13.5
12.6
12.0
10.7
10.1
9.0
6.8
4.9
3.0
1.6
0.94
absorbance
wavenumber (cm-1)
MA-68 Ar - no annealing
d.
15.7
13.0
11.4
10.0
8.1
6.5
4.2
absorbance
wavenumber (cm-1)

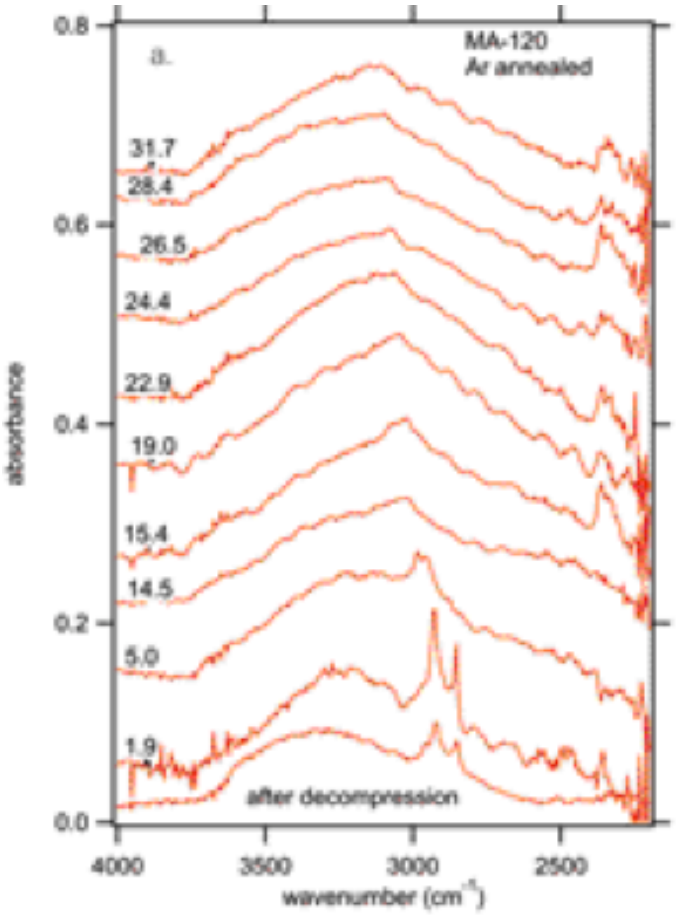
a.
MA-120
Ar annealed
31.7
28.4
26.5
24.4
22.9
19.0
15.4
14.5
5.0
1.9
after decompression
absorbance
wavenumber (cm-1)

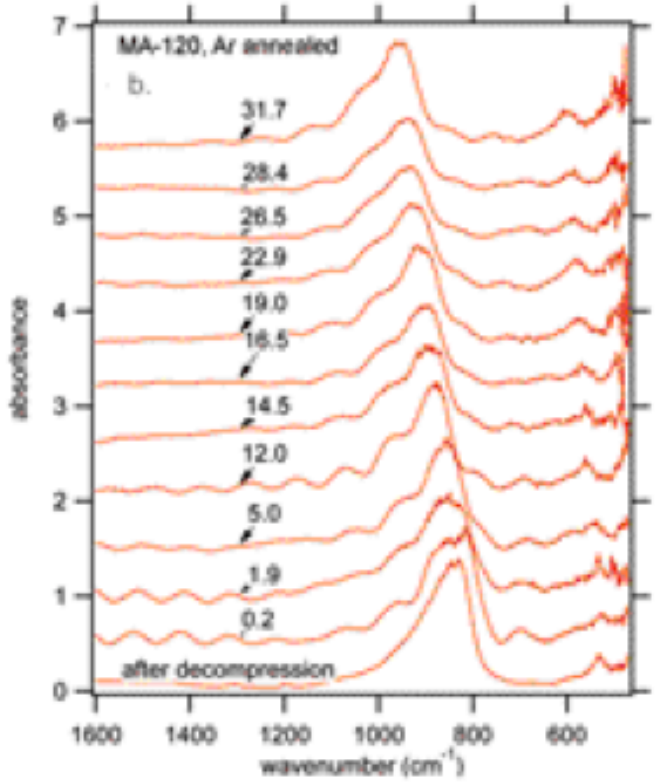
MA-120, Ar annealed
b.
31.7
28.4
26.5
22.9
19.0
16.5
14.5
12.0
5.0
1.9
0.2
after decompression
absorbance
wavenumber (cm-1)

FIG 4

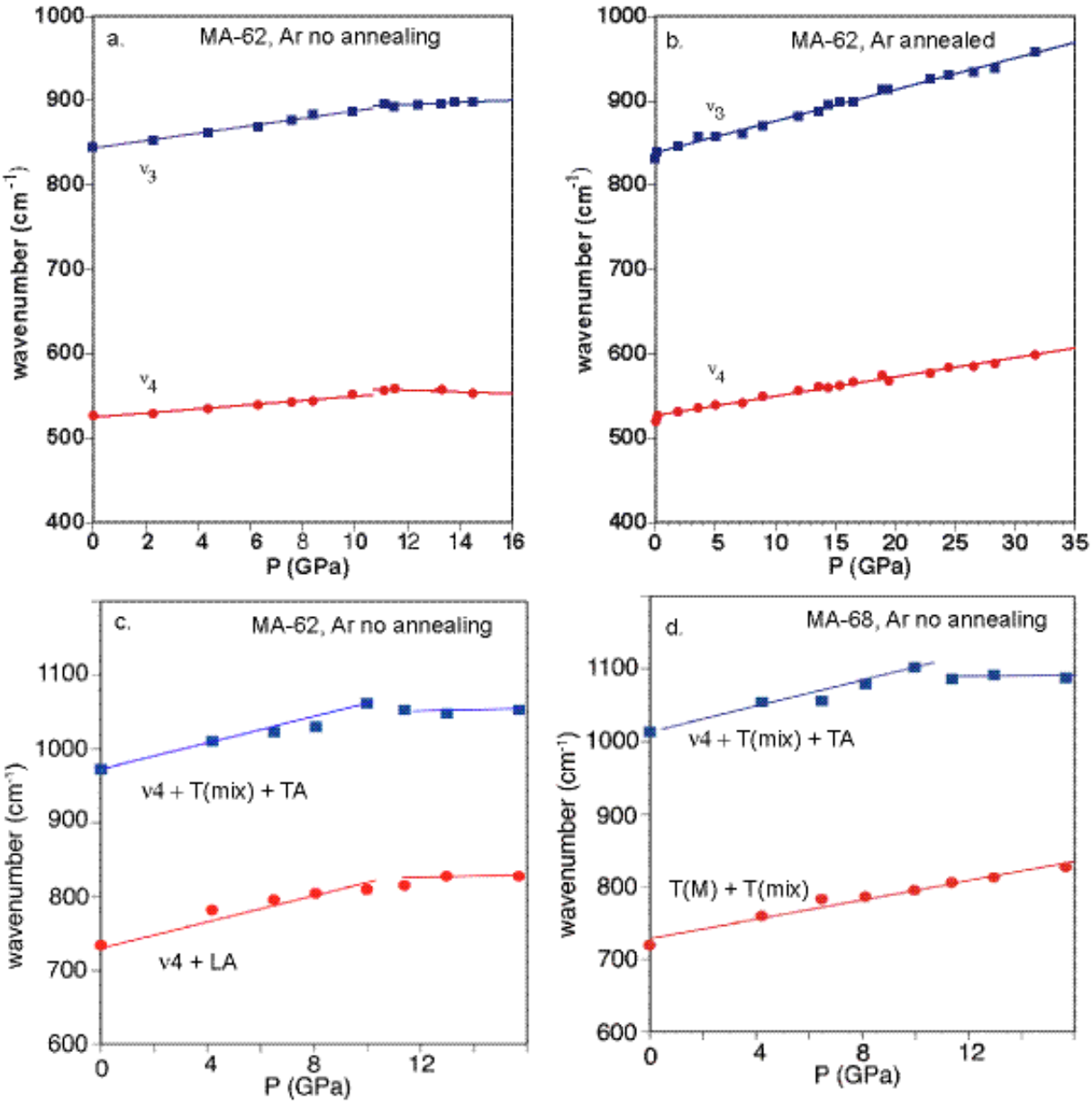
a.
MA-62, Ar no annealing
v3
v4
wavenumber (cm-1)
P (GPa)
b.
MA-62, Ar annealed
v3
v4
wavenumber (cm-1)
P (GPa)
c.
MA-62, Ar no annealing
v4 + T(mix) + TA
v4 + LA
wavenumber (cm-1)
P (GPa)
d.
MA-68, Ar no annealing
v4 + T(mix) + TA
T(M) + T(mix)
wavenumber (cm-1)
P (GPa)

Fig. 5

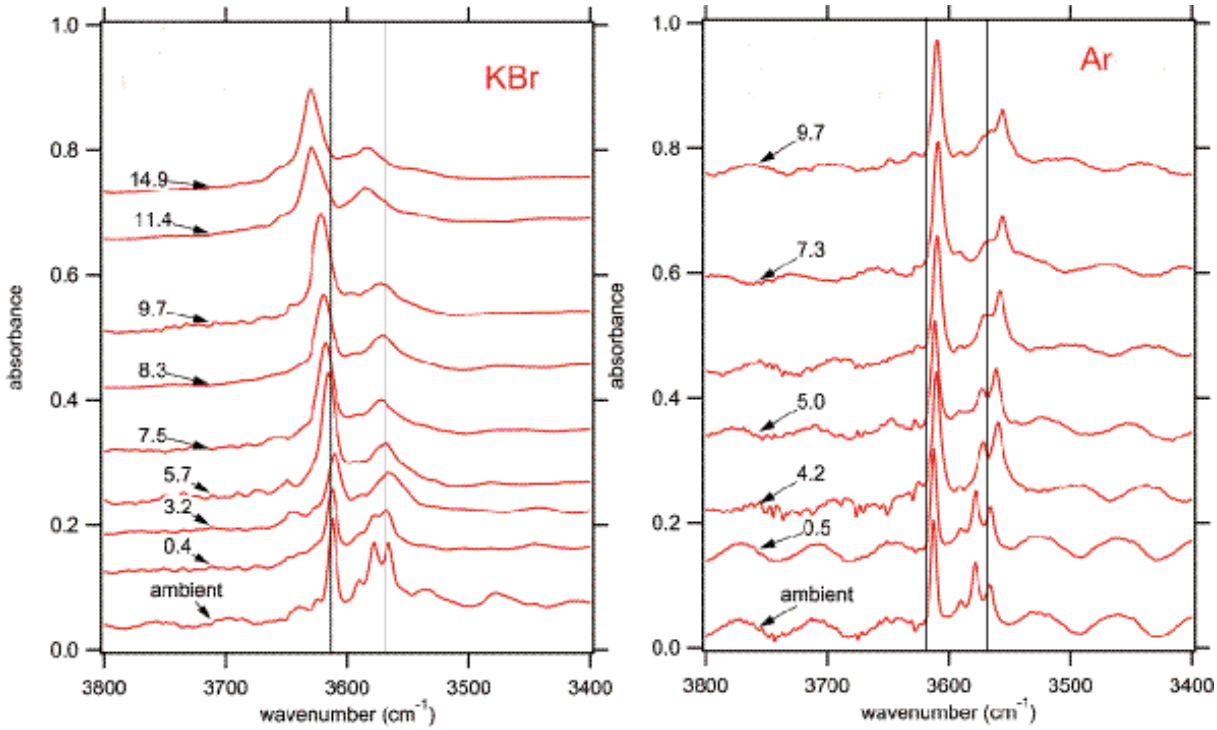
KBr
Ar
absorbance
wavenumber (cm^{-1})
14.9
11.4
9.7
8.3
7.5
5.7
3.2
0.4
ambient
9.7
7.3
5.0
4.2
0.5
ambient

Fig. 6